Biophysical Journal Volume 107 September 2014 1273–1279

Article

Hypercompliant Apical Membranes of Bladder Umbrella Cells

John C. Mathai,[1,*] Enhua H. Zhou,[2] Weiqun Yu,[1] Jae Hun Kim,[2] Ge Zhou,[3] Yi Liao,[3] Tung-Tien Sun,[3] Jeffrey J. Fredberg,[2] and Mark L. Zeidel[1]
[1]Department of Medicine, Beth Israel Deaconess Medical Center, Harvard Medical School and [2]Department of Environmental Health, Harvard School of Public Health, Boston, Massachusetts; and [3]Department of Cell Biology, New York University, New York, New York

ABSTRACT Urinary bladder undergoes dramatic volume changes during filling and voiding cycles. In the bladder the luminal surface of terminally differentiated urothelial umbrella cells is almost completely covered by plaques. These plaques (500 to 1000 nm) are made of a family of proteins called uroplakins that are known to form a tight barrier to prevent leakage of water and solutes. Electron micrographs from previous studies show these plaques to be interconnected by hinge regions to form structures that appear rigid, but these same structures must accommodate large changes in cell shape during voiding and filling cycles. To resolve this paradox, we measured the stiffness of the intact, living urothelial apical membrane and found it to be highly deformable, even more so than the red blood cell membrane. The intermediate cells underlying the umbrella cells do not have uroplakins but their membranes are an order of magnitude stiffer. Using uroplakin knockout mouse models we show that cell compliance is conferred by uroplakins. This hypercompliance may be essential for the maintenance of barrier function under dramatic cell deformation during filling and voiding of the bladder.

INTRODUCTION

Voiding disorders afflict millions and engender huge costs. Increasing evidence indicates that a significant proportion of the symptomatology of common bladder diseases such as cystitis (interstitial, chemical, or infectious) and lower urinary tract syndrome (LUTS) is caused by the failure of urothelial barrier function (1–4). Successful bladder filling, urine storage, and voiding requires an intact urothelium. At the urothelial surface, umbrella cells (UCs) maintain an exceptionally tight barrier between urine and blood, which features enormous chemical gradients between the urine on the apical side, and the blood on the basolateral side. Moreover, UCs maintain this barrier while undergoing dramatic shape changes from globular rectangles when the bladder is empty to flattened flagstones when the bladder is full. Such dramatic shape changes must require extraordinary mechanical resilience and compliance of the UCs. However, electron microscopy studies of UC apical membranes show 90% of the apical surface to be covered with plaque-like structures, where each plaque is composed of a family of four to five proteins called uroplakins (5). Freeze fracture studies further show that uroplakins are packed into paracrystalline arrays to form the hexagonal plaques covering the apical membrane (6,7). These plaques are visible on transmission and scanning electron microscopy and have been described in the UCs of all mammalian species studied to date (8). Indeed, the apparent rigidity of these plaques gives the luminal surface of the bladder its characteristic angular appearance in the electron micrographs, which led to the proteins that comprise them being named "uroplakins" (9,10). The paracrystalline organization in each plaque has led to the long-standing belief that those plaques comprise rigid structures (6,10). Such structural rigidity seems incompatible with the function of the urothelium, however, as the urothelium needs to stretch and flex as the bladder fills and empties. To resolve this paradox, in this study we report the first (to our knowledge) direct mechanical measurements of the urothelial apical surface stiffness (deformability) in intact, living, mouse urothelium.

To measure the stiffness of apical surface of the UCs in its native state, we used optical magnetic twisting cytometry (OMTC) (11–13). OMTC probes the local mechanical properties by attaching microscopic ferromagnetic beads (4.5 μm) to the urothelial surface and optically tracking forced bead motions through an inverted microscope during application of an oscillating magnetic field. To study the contribution of uroplakins to those properties, we used both wildtype and uroplakin-knockout mice. Because submembrane actin networks are known to modulate cell rigidity (14,15), we labeled normal and uroplakin null urothelia to determine the extent of subapical actin networks. Our results suggest that the high deformability of the UC apical membrane is attributable both to the presence of uroplakin paracrystalline arrays and the lack of a subapical actin network. The high pliability of the apical surface may enhance its mechanical stability allowing it to maintain tight barrier function in the face of large changes in bladder volume.

Submitted December 19, 2013, and accepted for publication July 22, 2014.
*Correspondence: jmathai@bidmc.harvard.edu
John C Mathai, Enhua H. Zhou and Weiqun Yu contributed equally to this work.
Enhua H. Zhou's present address is Ophthalmology, Novartis Institutes of BioMedical Research, Cambridge, Massachusetts.
Editor: Gijsje Koenderink

0006-3495/14/09/1273/7 $2.00
http://dx.doi.org/10.1016/j.bpj.2014.07.047

MATERIALS AND METHODS

Bladder tissue preparation and cell culture for OMTC and atomic force microscopy

Mice were euthanized by inhalation of 100% CO_2. After euthanasia and thoracotomy, the bladders were rapidly excised and processed as described below. All animal studies were performed in adherence to U.S. National Institutes of Health guidelines for animal care and use and with the approval of the Beth Israel Deaconess Medical Center Institutional Animal Care and Use Committee. The freshly harvested bladders were cut open longitudinally, mounted on a circular Teflon holder for OMTC or a homemade transparent -Polydimethylsiloxane (PDMS) pad for atomic force microscopy (AFM). In both cases, the samples are immersed in Krebs solution and treated with 10 μM atropine and 15 μM 5'-(N-ethylcarboxamido) adenosine (NECA) for 30 min to reduce the spontaneous movement of the bladder tissue. In some experiments, to remove the UCs, the samples were further treated with protamine sulfate (10 mg/ml) for 15 min and then washed with Krebs solution. Magnetic beads were then added to the luminal side of the bladder for OMTC measurements (see below). Madin-Darby canine kidney epithelial (MDCK) cells (strain II) were cultured in Dulbecco's Modified Eagle's Medium (DMEM) with 10% Fetal bovine serum (FBS) to confluence, and switched to serum-free media before OMTC measurements. Red blood cells (RBCs) were obtained from a healthy donor by a fingertip needle prick, washed, suspended in phosphate buffered saline (PBS), and attached to a poly-L-lysine coated plastic before OMTC measurements (16).

OMTC

The experimental setup for OMTC measurements has been described in detail elsewhere (11,12). Briefly, 4.5 μm ferromagnetic beads were coated with poly-L-lysine (PLL; 4 kDa) at 75 μg PLL/mg beads. In contrast to other extracellular matrix ligands such as fibronectin or RGD peptide, PLL coating does not activate integrins and or induce focal adhesion formation and yet allows avid binding of the magnetic beads to the cell cortex, producing similar cell stiffness measurements as compared with RGD-coated beads (17). After attachment of the beads to sample surface for 30 min at 37°C, the sample was gently washed to remove the unbound beads and was placed on the stage of an inverted microscope (Leica Model #DM IRBE, Leica Microsystems, Wetzlar, Germany) and viewed under bright-field with a 10× objective. The beads were then magnetized horizontally and twisted vertically by an external homogeneous magnetic field that varied sinusoidally in time. Lateral bead displacement in response to the resulting oscillatory torque was detected by a charge-coupled device camera (JAI CV-M10) mounted on the inverted microscope. Images were analyzed using an intensity-weighted center-of-mass algorithm to determine bead position with an accuracy of 5 nm. The specific torque, T, is the mechanical torque per bead volume and has the dimension of stress (Pa). The ratio of the complex specific torque $\widetilde{T}$ to the resulting complex bead displacement $\widetilde{d}$ defines a complex elastic modulus, $\widetilde{G} = \widetilde{T}(f)/\widetilde{d}(f)$. For each bead, we computed the apparent modulus ($|\widetilde{G}|$), which has the unit of Pa/nm. To convert the apparent modulus to shear modulus, we multiplied it by a geometric factor of 6800 nm, based on previous finite-element simulations (18) and the assumption that 10% of the bead height is embedded in the cell (12). All data were analyzed using custom software written using Matlab. Error bars are standard errors (n = 42 to 120 beads on two to six bladders, n = ~ 91 cells for MDCK cells, and n = ~ 120 cells for RBCs, $P < 0.001$ between wildtype and uroplakin II knockout bladders).

AFM measurements

AFM measurements were performed using the protocol described by Kim et al. (19). The apical surface of the urothelium was probed using a borosilicate spherical tip with a nominal diam. of 5 μm. The nominal spring constant was $k = 0.06$ N/m (Novascan Technologies, Ames, IA) and calibrated before use. Indentation was carried out using a commercial AFM (MFP-3D; Asylum, Santa Barbara, CA). We computed the shear modulus of urothelium by fitting the force-depth curves over a range of depths (800 nm), using the Hertz model (20) (see Fig. 3). Initial contact between a sphere and the bladder surface was determined by root mean square (RMS) error analysis (19) (see inset in Fig. 3). Fifty force-depth curves were collected from three mouse bladders. On the surface of each bladder, indentations were separated laterally by at least 10 μm. Measurements were completed within 5 h of tissue removal from mice. Maximum forces were ~ 1.6 nN. For the urothelium, a Poisson's ratio of 0.5 was used to recover shear modulus.

Measurement of urothelial barrier function

Animal experiments were performed in accordance with the animal use and care committees of New York University, University of Pittsburgh, and Beth Israel Deaconess Medical Center. Bladders were excised after lethal anesthesia, washed in placed in NaCl-Ringer buffer (110 mM NaCl, 5.8 mM KCl, 25 mM NaHCO3, 1.2 mM KH2PO4, 2.0 mM CaCl2, 1.2 mM MgSO4, and 11.1 mM glucose (pH 7.4) at 37°C, bubbled with 95% O_2, 5% CO_2 gas) and carefully stretched and mounted on a small ring in the same solution at 37°C. The bladder was then placed in a modified Ussing chamber (21). Both compartments of the chamber were under constant stirring and temperature control, while allowing electrical measurements and sampling.

In all other transepithelial resistance measurements both voltage-sensing and current-passing electrodes were connected to an automatic voltage clamp (EC-825, Warner Instruments, Hamden, CT), which was, in turn, connected to a microcomputer with a MacLab interface (21,22). All permeability measurements were performed at 37°C after stabilization of the transepithelial resistance. Diffusive water and urea permeability coefficients were determined by using isotopic fluxes as described (21,23). Briefly, tritiated water (1 μCi/ml) or [14C] urea (0.25 μCi/ml) were added to the apical chamber and 100 μl samples of both apical and basolateral chambers were taken every 15 min. Sample volumes were replaced quantitatively with warmed NaCl-Ringer. Sample radioactivities were counted with a liquid scintillation counter (model 1500, Packard Tri-Carb, Waltham, MA), and flux rates and permeabilities were calculated as described previously (21,23). In Fig. 1, six to eight mice were used for the first time point and 10 to 15 mice each for rest of the time points.

Confocal microscopy

Bladders were fixed with 4% paraformaldehyde in 100 mM cacodylate as described in an earlier study (24). Using a Leica CM1850 cryostat, sections 4 μm thick were cut and prepared for immunofluorescence staining. Staining was done for 60 min with rhodamine-phalloidin (1:50), and Topro-3 (1:1,000) after quench and permeabilization (0.1% Triton X100, 75 mM NH_4Cl, 20 mM glycine, Phosphate buffered saline, pH7.4.), and then blocking (0.5% fish gelatin, 25 mM saponin, 20 mM Na azide, PBS). Confocal microscopy was performed on an LSM 510 META confocal microscope (Carl Zeiss MicroImaging, Inc., Jena, Germany) using a 63× oil immersion objective. Serial Z section images were obtained with each focal plane images acquired three times and averaged to reduce noise. Every attempt was made to collect and process images in an identical manner. Images were imported into Velocity 3D Image Analysis Software 6. 2. 1 for F-actin fluorescent intensity analysis. Mean fluorescent intensity per unit volume for sub-apical and basal F-actin network was obtained. TIFF format images were finally imported into Adobe illustrator 6.0 (Adobe Corp., San Jose, CA). To insure that observed changes were not affected by artifacts, samples from control and experimental groups were fixed in an identical manner and examined under identical conditions of magnification, light intensity, etc. Similar results from three different bladders from a given experimental or control group are considered sufficient for drawing conclusions.

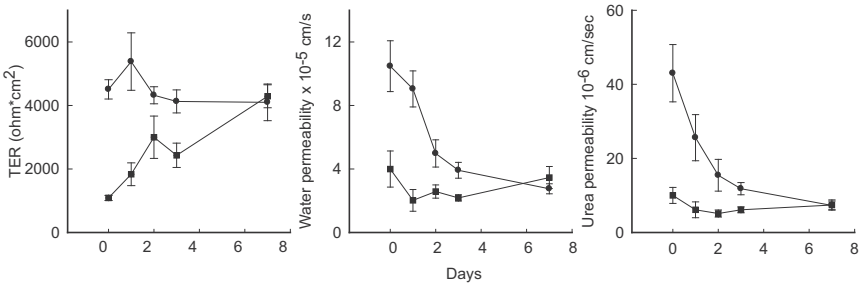

FIGURE 1 Removal of UCs using protamine leads to disruption of bladder barrier function. Time course of effects of PBS or protamine sulfate instilled in the mice bladder shows bladder function as measured by transepithelial resistance (TER; *left panel*), water (*middle panel*), and urea permeability (*right panel*) is restored to basal levels within 6 days of protamine sulfate (10 mg/ml) instillation in the mice bladder (n of 6 to 15 mice, standard error shown). Squares and circles denote normal (PBS instilled) and injured (protamine instilled) urothelium respectively (* $P < 0.05$, between normal and protamine treated, 1 h after protamine installation).

Uroplakin II knockout mice

Knockout of uroplakin II (UPII KO) ablates nearly all uroplakin expression in resulting UPII KO mice. We have previously shown that bladders of UPIII KO mice exhibit normal, high transepithelial resistances, but abnormally high water and urea permeabilities. Similarly the double knock $UPII^{-}/UPIII^{-}$ mice also show similar results. These mice have been described in earlier studies (22,25–27).

Protamine sulfate treatment of urothelium

Either 10 mg/ml of protamine sulfate (PS) diluted into PBS or PBS alone was instilled transurethrally into the bladder for 15 min while the animal was maintained under light halothane anesthesia and maintained for 15 min in the bladder before emptying. At varying time points after PS or PBS exposure, the animals were euthanized and the bladders were excised and mounted in Ussing chambers for resistance and permeability measurements as described in an earlier study (27).

RESULTS

Characterization of a model of UC removal with PS

We and others have previously described the use of PS to remove nearly all of the surface UCs and abruptly exposing underlying intermediate cells to the surface (22,27,28). In rats, abrupt removal of the UC layer results in immediate striking increases in water and urea permeabilities and a drop in transepithelial resistance. By day 6, these barrier functions, (transepithelial resistance and water and urea permeability values) have returned to normal, and persisted at normal levels for weeks. Interestingly the size of the cell remains small until day 10 after which it is restored (29). Fig. 1 shows similar results in mice. Protamine exposure leads to prompt loss of barrier function, which is restored in 6 days.

Measurement of apical membrane deformability by OMTC

OMTC has been applied to numerous cell types to measure their mechanical properties (12,30,31), glassy dynamics of the cytoskeleton (12,13,17), fluidization and resolidification responses to stretch (13,32), stiffening responses to compression (17), and contractile responses to pharmacological agents (33–35). Using this technique the stiffness of the apical membrane of the bladder was calculated by computing the elastic shear modulus based on the lateral displacement of magnetic beads that are attached to surface of the bladder in response to an imposed magnetic field. Fig. 2 compares the deformability of control UC, intermediate cells (after protamine removal of UCs), and UCs after paraformaldehyde fixation. These values are also compared with those of RBCs and cultured MDCK cells.

Normal mouse urothelium exhibited a strikingly small shear modulus (G was evaluated at 0.77 Hz to be 31 $\pm$ 3.5 Pa; n = 98 beads on six bladders; all data reported as average $\pm$ SE), even smaller than that of the highly deformable RBCs (87 $\pm$ 6.4 Pa; n = ~ 120 cells). As expected, fixation of the bladder tissue with paraformaldehyde led to marked stiffening of the urothelial surface (5168 $\pm$ 1018 Pa; n = 42 beads on two bladders). Interestingly, 30 min after the urothelium was denuded of UCs using protamine, the formerly underlying and now newly exposed intermediate cells exhibit a relatively high level of stiffness (389 $\pm$ 64 Pa; n = 72 beads on three bladders) resembling that of cultured renal epithelial (MDCK) cells (583 $\pm$ 57 Pa; n = ~ 91 cells). UPII KO UCs lacking uroplakins exhibited a stiffness value of 82 $\pm$ 9 Pa (n = 79 beads on four bladders), which is nearly three times that of wildtype.

Confirmation of high deformability of UCs with AFM

Although the OMTC method has been used extensively to characterize the rheology of many cell types including erythrocytes (16,36) and MDCK (17) cells, the reported values of shear modulus of urothelium was smaller than that of erythrocytes that are highly deformable. To confirm that the small shear modulus of UC as measured by OMCT is not a measurement artifact, we also used AFM, which is independent of bead attachment. Previous studies showed a good agreement between OMTC and AFM measurements on A549 epithelial cells (37,38). AFM employs a highly sensitive cantilever to indent the surface of bladder, giving rise to reaction forces that are measured as a function of the indentation depth. The sheer modulus of the surface is computed directly from the force-indentation depth curves

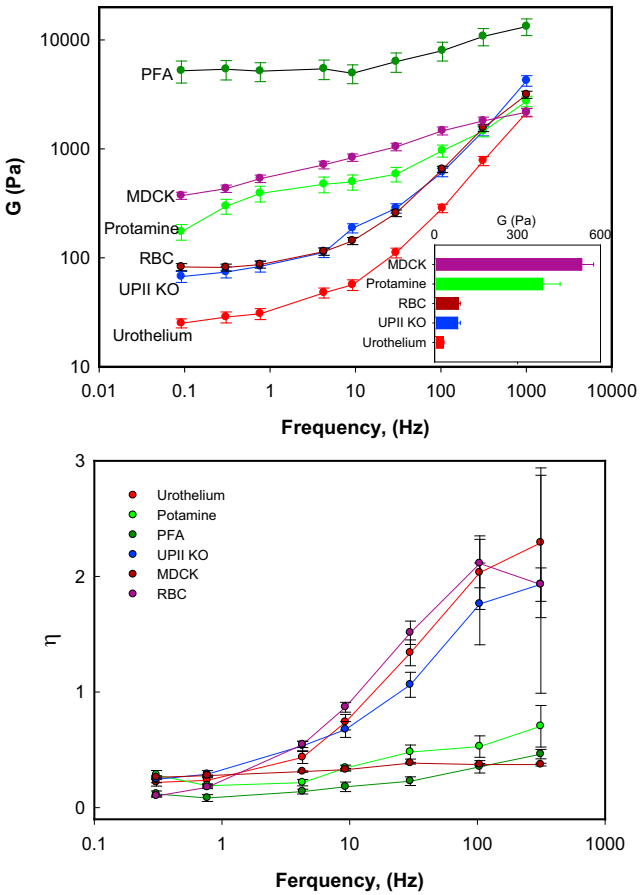

FIGURE 2 The native wildtype urothelium displays extraordinary membrane compliance. Elastic modulus was measured by OMTC (see Methods). Top panel: native urothelium containing uroplakin plaques on the apical surface exhibit very low G, indicating a very high deformability. The bladders of uroplakin II KO mice that are devoid of uroplakins on the surface show an enhanced stiffness similar to that of a red blood cell (RBC). The stiffness of intermediate cells exposed by protamine treatment is similar to that of MDCK cells. Bladders exposed to paraformaldehyde (PFA), as expected, show significantly increased stiffness. Inset shows stiffness values at 0.77 Hz as a bar graph. The value for PFA (5168 Pa) is not shown in the inset. Bottom panel shows the dissipation data η, the ratio between loss modulus and storage modulus.

(19). AFM measurements performed on intact control mouse urothelium, shown in Fig. 3, confirmed the high deformability of the urothelial surface. We obtained a shear modulus of ~ 180 ± 6 Pa (n = 3 bladders) from AFM measurements, which is within an order of magnitude of that obtained from OMTC. This degree of concordance is consistent with the notion that AFM versus OMTC couple to the cell in a different manner, in a different geometry, and therefore impose very different types of deformations; as a result, OMTC probes local deformability of the apical membrane whereas AFM probes the combined properties of apical membrane, cytoskeletal network, and cytoplasm beneath the apical surface of the cell. For instance, a typical cultured MDCK cell is an order of magnitude stiffer, averaging 583 Pa

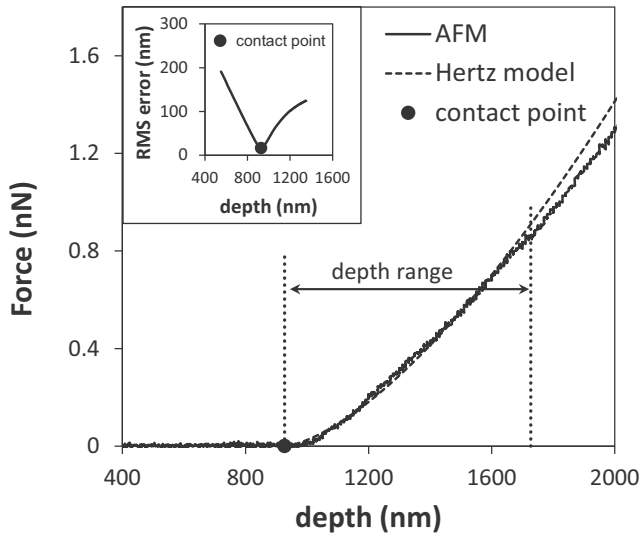

FIGURE 3 AFM measurement confirmed the membrane hypercompliance of the bladder UCs. Representative force-indentation curve of a normal mouse urothelium shows good agreement with the Hertz elastic model, allowing extraction of the shear modulus computed over a range of depths (800 nm). Depth range and contact point are marked as dotted lines and a dot, respectively. The depth that minimized RMS error was taken as contact point (inset). The shear modulus of UCs in situ was found to be 180 ± 6 Pa (n = 3 bladders, mean ± SD, 18 to 27 measurements were performed on each bladder).

when probed using OMTC and close to 2000 Pa when probed using AFM (39). These AFM measurements confirm that the low shear modulus exhibited by UC apical surface by OMTC is not an artifact.

Role of subapical F-Actin networks in apical membrane deformability

In other tissues F-actin networks under the membrane bind to membrane proteins, and provide structural stability and rigidity to the overlying membrane (14). It is also established that F-actin is the major determinant of the stiffness of cells in culture (15). To determine the role of F-actin networks in UC surface deformability, we labeled native UCs and UCs lacking uroplakins with phalloidin. We visualized the spatial distribution of F-actin on apical and basal side of the same cell using confocal microscopy. As shown in Fig. 4, wildtype UCs had very little or no detectable F-actin network under their apical membranes. Labeling for uroplakins using uroplakin antibodies show abundant presence of uroplakins in the UCs. Interestingly, uroplakin knockout UCs had more F-actin in their apical membrane than control UCs. The diminished uroplakin level in uroplakin knockout is associated with increased apical F-actin content as well as decreased cell deformability. Uroplakin thus appears to serve the dual functions of reducing apical membrane permeability and increasing its deformability.

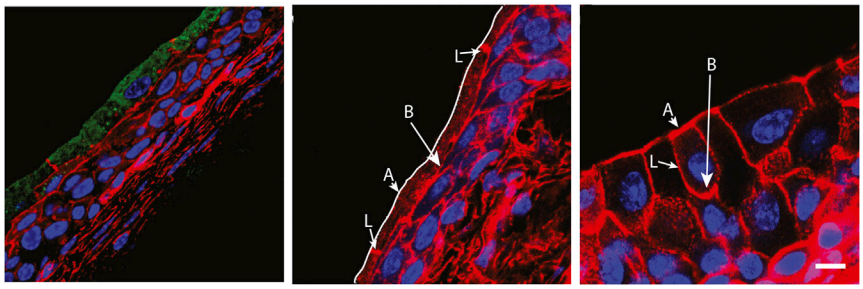

FIGURE 4 F-actin labeling of wildtype and UPII KO urothelium. Left panel shows uroplakin label (*green*) and actin labeling in red in wildtype. Uroplakin is only found in top most UCs, which can be as large as ~ 100 μm compared with the cells underneath it. Because of its large size, a nuclei is not always seen in the sections. There is negligible actin labeling in the apical membrane of the UCs. The middle panel shows only actin labeling in wildtype and the apical membrane is traced in white as its outlines are not clearly visible because of lack of actin. The right panel shows urothelium of UPII KO lacking uroplakins, where the topmost cells are uniformly smaller (20 to 30 μm) and actin distribution is similar in apical and basal membranes. A, apical; B, basal; and L, lateral sides of the cell. The scale bar is 10 μm.

DISCUSSION

Although barrier function appears to be a major specialized property of UCs, they must maintain this barrier function as they change shape from ovaloid blobs when the bladder is empty to flat flagstones when it is full. How UCs achieve these remarkable shape changes is unknown. The mechanisms involved have been unclear because earlier electron microscopic studies show uroplakin protein arrays to be rigid discs or plaques connected to each other by thinner membranes, or so-called "hinge" regions (9,10).

The paradox of an epithelial cell that can deform enormously yet features an apical membrane composed almost entirely of rigid plaques might be resolved in part by an endocytic-exocytic mechanism for changing the apical membrane surface area. Indeed, early studies noted that the numbers of plaques in endosomes rose dramatically as the bladder emptied, and declined sharply as it filled (40,41). However, this may be a mechanism for increasing the surface area of the cell rather than just shape change during bladder filling and emptying. It is also possible that such a tightly packed rigid structure might be needed to achieve the exceptionally low permeabilities of the UC apical membrane.

Our shear modulus measurements using both OMTC and AFM techniques show that control UC apical membranes exhibit enormous deformability, surpassing that of RBCs, which, of course, must squeeze through slender capillaries as they circulate. UC apical membranes were far more deformable than the apical membranes of cultured renal epithelial cells. Importantly, removal of the UC layer and exposure of intermediate cells to the surface revealed that intermediate cell apical membranes are far less deformable than those of UCs.

The OMTC method to determine the shear modulus of the cells involves the assumption that 10% of the bead height is embedded in the cell. Although this assumption remains to be validated by three-dimensional imaging for both the wild-type and uroplakin knockout mice, OMTC has come to be widely accepted in cell rheology (42). The degree of embedding is heterogeneous even for a monolayer of same cell type and is difficult to quantify (43). A 10% bead embedment was shown to give stiffness values comparable with that obtained using other techniques such as AFM and optical tweezers (18,43). Given this caveat, our finding that UPII KO UCs are stiffer than their wild counterparts was consistent with the F-actin staining results. In addition, the low shear modulus obtained using OMTC was consistent with that obtained using AFM to within an order of magnitude, adding confidence to our OMTC measurements.

To determine how UC apical membranes achieve such a high level of deformability, we examined two likely candidate mechanisms. The first possibility is that uroplakins, which cover almost the entire apical membrane and which are sparse in intermediate cells, might provide the deformable structure of the apical membrane. If this were true, this represents an important insight into a novel uroplakin function, in addition to contributing to the formation of a highly impermeable urothelial surface. The second possibility is that the F-actin cytoskeletal network, which underlies many membranes, may be absent or poorly developed under the UC apical membrane. This explanation is attractive because cortical actin thickness of a cell was shown to directly correlate with cell stiffness (14).

To test these possibilities, we repeated our measurements on uroplakin knockout mice. Ablation of uroplakins led to a level of deformability between that of the native UC and the intermediate cell (Fig. 2). F-actin labeling of control UCs shows abundant labeling of underlying basolateral membrane domains, but nearly none underlying apical membrane domains (Fig. 4). Interestingly, UCs lacking uroplakin exhibited higher F-actin labeling patterns than those of the intermediate cells and control UCs. These results suggest that both the presence of uroplakins and lack of an actin network underlying the UC apical membrane contribute to maintaining high apical surface deformability in native UCs. We cannot rule out the possibility of cytoskeletal rearrangement or remodeling in these cells chronically lacking uroplakins.

If high apical membrane deformability represents an important differentiated trait of the fully mature UC, then it is possible that the lack of deformability of intermediate cells after urothelial injury as modeled in protamine

treatment results in an inability of the urothelial layer to maintain barrier function in the face of stretch and relaxation. Indeed, humans with urothelial injury exhibit frequency and urgency, suggesting a failure of the permeability barrier. Similarly UPII KO mice showed increased bladder capacity, micturition pressure, and nonvoiding contractions (26,44). Although UCs maintain permeability barrier, the bladder filling and voiding also involves coordinated control of the bladder musculature and the bladder and urethral sphincter.

In summary we have measured for the first time (to our knowledge) the deformability of the UC apical membrane. Despite the preponderance of numerous, rigid-appearing plaques in fixed UCs on electron microscopy, the UC apical membrane is remarkably deformable. Uroplakins appear to play an important role in the high deformability of UC apical membranes, which is likely an intrinsic intracellular mechanical property of the uroplakins.

We thank Ms. Susan Meyers for technical help.

AFM measurements were performed at Harvard Center for Nanoscale Systems (CNS), a member of the National Nanotechnology Infrastructure Network (NNIN), which is supported by the National Science Foundation under NSF award No. ECS-0335765. A NIH grant No. 1P01HL120839 was awarded to J.F. and the work in T.-T. Sun's lab was supported by grants from NIH (DK52206, DK39753).

REFERENCES

1. Buffington, C. A., J. L. Blaisdell, …, B. E. Woodworth. 1996. Decreased urine glycosaminoglycan excretion in cats with interstitial cystitis. *J. Urol.* 155:1801–1804.
2. Elbadawi, A. E., and J. K. Light. 1996. Distinctive ultrastructural pathology of nonulcerative interstitial cystitis: new observations and their potential significance in pathogenesis. *Urol. Int.* 56:137–162.
3. Lavelle, J. P., S. A. Meyers, …, G. Apodaca. 2000. Urothelial pathophysiological changes in feline interstitial cystitis: a human model. *Am. J. Physiol. Renal Physiol.* 278:F540–F553.
4. Graham, E., and T. C. Chai. 2006. Dysfunction of bladder urothelium and bladder urothelial cells in interstitial cystitis. *Curr. Urol. Rep.* 7:440–446.
5. Wu, X. R., X. P. Kong, …, T. T. Sun. 2009. Uroplakins in urothelial biology, function, and disease. *Kidney Int.* 75:1153–1165.
6. Staehelin, L. A., F. J. Chlapowski, and M. A. Bonneville. 1972. Lumenal plasma membrane of the urinary bladder. I. Three-dimensional reconstruction from freeze-etch images. *J. Cell Biol.* 53:73–91.
7. Kachar, B., F. Liang, …, T. T. Sun. 1999. Three-dimensional analysis of the 16 nm urothelial plaque particle: luminal surface exposure, preferential head-to-head interaction, and hinge formation. *J. Mol. Biol.* 285:595–608.
8. Wu, X. R., J. H. Lin, …, T. T. Sun. 1994. Mammalian uroplakins. A group of highly conserved urothelial differentiation-related membrane proteins. *J. Biol. Chem.* 269:13716–13724.
9. Wu, X. R., M. Manabe, …, T. T. Sun. 1990. Large scale purification and immunolocalization of bovine uroplakins I, II, and III. Molecular markers of urothelial differentiation. *J. Biol. Chem.* 265:19170–19179.
10. Hicks, R. M. 1975. The mammalian urinary bladder: an accommodating organ. *Biol. Rev. Camb. Philos. Soc.* 50:215–246.
11. Bursac, P., B. Fabry, …, S. S. An. 2007. Cytoskeleton dynamics: fluctuations within the network. *Biochem. Biophys. Res. Commun.* 355:324–330.
12. Fabry, B., G. N. Maksym, …, J. J. Fredberg. 2001. Scaling the microrheology of living cells. *Phys. Rev. Lett.* 87:148102.
13. Trepat, X., L. Deng, …, J. J. Fredberg. 2007. Universal physical responses to stretch in the living cell. *Nature.* 447:592–595.
14. MacQueen, L. A., M. Thibault, …, M. R. Wertheimer. 2012. Electromechanical deformation of mammalian cells in suspension depends on their cortical actin thicknesses. *J. Biomech.* 45:2797–2803.
15. Wang, N., J. P. Butler, and D. E. Ingber. 1993. Mechanotransduction across the cell surface and through the cytoskeleton. *Science.* 260: 1124–1127.
16. Puig-de-Morales-Marinkovic, M., K. T. Turner, …, S. Suresh. 2007. Viscoelasticity of the human red blood cell. *Am. J. Physiol. Cell Physiol.* 293:C597–C605.
17. Zhou, E. H., X. Trepat, …, J. J. Fredberg. 2009. Universal behavior of the osmotically compressed cell and its analogy to the colloidal glass transition. *Proc. Natl. Acad. Sci. USA.* 106:10632–10637.
18. Mijailovich, S. M., M. Kojic, …, J. J. Fredberg. 2002. A finite element model of cell deformation during magnetic bead twisting. *J. Appl. Physiol.* 93:1429–1436.
19. Kim, J. H., J. P. Butler, and S. H. Loring. 2011. Probing softness of the parietal pleural surface at the micron scale. *J. Biomech.* 44:2558–2564.
20. Hertz, H. 1882. Über die Berührung fester elastischer Körper (on the contact of elastic solids). *Journal fur die Reine und Angewandte Mathematik.* 92:156–171.
21. Negrete, H. O., J. P. Lavelle, …, M. L. Zeidel. 1996. Permeability properties of the intact mammalian bladder epithelium. *Am. J. Physiol.* 271:F886–F894.
22. Hu, P., S. Meyers, …, T. T. Sun. 2002. Role of membrane proteins in permeability barrier function: uroplakin ablation elevates urothelial permeability. *Am. J. Physiol. Renal Physiol.* 283:F1200–F1207.
23. Lavelle, J. P., G. Apodaca, …, M. L. Zeidel. 1998. Disruption of guinea pig urinary bladder permeability barrier in noninfectious cystitis. *Am. J. Physiol.* 274:F205–F214.
24. Acharya, P., J. Beckel, …, G. Apodaca. 2004. Distribution of the tight junction proteins ZO-1, occludin, and claudin-4, -8, and -12 in bladder epithelium. *Am. J. Physiol. Renal Physiol.* 287:F305–F318.
25. Hodges, S. J., G. Zhou, …, G. J. Christ. 2008. Voiding pattern analysis as a surrogate for cystometric evaluation in uroplakin II knockout mice. *J. Urol.* 179:2046–2051.
26. Kong, X. T., F. M. Deng, …, T. T. Sun. 2004. Roles of uroplakins in plaque formation, umbrella cell enlargement, and urinary tract diseases. *J. Cell Biol.* 167:1195–1204.
27. Zocher, F., M. L. Zeidel, …, J. C. Mathai. 2012. Uroplakins do not restrict CO2 transport through urothelium. *J. Biol. Chem.* 287: 11011–11017.
28. Tzan, C. J., J. Berg, and S. A. Lewis. 1993. Effect of protamine sulfate on the permeability properties of the mammalian urinary bladder. *J. Membr. Biol.* 133:227–242.
29. Lavelle, J., S. Meyers, …, M. L. Zeidel. 2002. Bladder permeability barrier: recovery from selective injury of surface epithelial cells. *Am. J. Physiol. Renal Physiol.* 283:F242–F253.
30. Bursac, P., G. Lenormand, …, J. J. Fredberg. 2005. Cytoskeletal remodelling and slow dynamics in the living cell. *Nat. Mater.* 4:557–561.
31. Deng, L., X. Trepat, …, J. J. Fredberg. 2006. Fast and slow dynamics of the cytoskeleton. *Nat. Mater.* 5:636–640.
32. Chen, C., R. Krishnan, …, J. J. Fredberg. 2010. Fluidization and resolidification of the human bladder smooth muscle cell in response to transient stretch. *PLoS ONE.* 5:e12035.
33. An, S. S., R. E. Laudadio, …, J. J. Fredberg. 2002. Stiffness changes in cultured airway smooth muscle cells. *Am. J. Physiol. Cell Physiol.* 283:C792–C801.
34. Laudadio, R. E., E. J. Millet, …, J. J. Fredberg. 2005. Rat airway smooth muscle cell during actin modulation: rheology and glassy dynamics. *Am. J. Physiol. Cell Physiol.* 289:C1388–C1395.

35. Zhou, E. H., R. Krishnan, …, M. Johnson. 2012. Mechanical responsiveness of the endothelial cell of Schlemm's canal: scope, variability and its potential role in controlling aqueous humour outflow. *J. R. Soc. Interface.* 9:1144–1155.

36. Marinkovic, M., M. Diez-Silva, …, J. P. Butler. 2009. Febrile temperature leads to significant stiffening of Plasmodium falciparum parasitized erythrocytes. *Am. J. Physiol. Cell Physiol.* 296:C59–C64.

37. Trepat, X., M. Grabulosa, …, D. Navajas. 2005. Thrombin and histamine induce stiffening of alveolar epithelial cells. *J. Appl. Physiol.* 98:1567–1574.

38. Alcaraz, J., L. Buscemi, …, D. Navajas. 2003. Microrheology of human lung epithelial cells measured by atomic force microscopy. *Biophys. J.* 84:2071–2079.

39. Hoh, J. H., and C. A. Schoenenberger. 1994. Surface morphology and mechanical properties of MDCK monolayers by atomic force microscopy. *J. Cell Sci.* 107:1105–1114.

40. Yu, W., P. Khandelwal, and G. Apodaca. 2009. Distinct apical and basolateral membrane requirements for stretch-induced membrane traffic at the apical surface of bladder umbrella cells. *Mol. Biol. Cell.* 20:282–295.

41. Khandelwal, P., S. N. Abraham, and G. Apodaca. 2009. Cell biology and physiology of the uroepithelium. *Am. J. Physiol. Renal Physiol.* 297:F1477–F1501.

42. Guo, M., A. J. Ehrlicher, …, D. A. Weitz. 2013. The role of vimentin intermediate filaments in cortical and cytoplasmic mechanics. *Biophys. J.* 105:1562–1568.

43. Laurent, V. M., S. Hénon, …, F. Gallet. 2002. Assessment of mechanical properties of adherent living cells by bead micromanipulation: comparison of magnetic twisting cytometry vs optical tweezers. *J. Biomech. Eng.* 124:408–421.

44. Aboushwareb, T., G. Zhou, …, G. J. Christ. 2009. Alterations in bladder function associated with urothelial defects in uroplakin II and IIIa knockout mice. *Neurourol. Urodyn.* 28:1028–1033.